Key Points:
- Martian ripples are diverse in morphology, dynamics, and activity
- Large Martian ripples belong to a family of bedforms that forms when a significant fraction of sediment transport occurs near the bed
- Near-bed-transport bedforms are found across environments and planets and may prove useful quantitative paleoenvironment indicators

Supporting Information:
- Supporting Information S1

Correspondence to:
M. G. A. Lapotre,
mlapotre@fas.harvard.edu

Morphologic Diversity of Martian Ripples: Implications for Large-Ripple Formation

M. G. A. Lapotre[1] [iD], R. C. Ewing[2] [iD], C. M. Weitz[3] [iD], K. W. Lewis[4] [iD], M. P. Lamb[5] [iD], B. L. Ehlmann[5,6] [iD], and D. M. Rubin[7]

[1]Department of Earth and Planetary Sciences, Harvard University, Cambridge, MA, USA, [2]Department of Geology and Geophysics, Texas A&M University, College Station, TX, USA, [3]Planetary Science Institute, Tucson, AZ, USA, [4]Department of Earth and Planetary Sciences, Johns Hopkins University, Baltimore, MD, USA, [5]Division of Geological and Planetary Sciences, California Institute of Technology, Pasadena, CA, USA, [6]Jet Propulsion Laboratory, California Institute of Technology, Pasadena, CA, USA, [7]Department of Earth and Planetary Sciences, University of California Santa Cruz, Santa Cruz, CA, USA

Abstract Large ripples with meter-scale wavelengths are ubiquitous across Mars. *Curiosity*'s traverse of the Bagnold Dune Field revealed a morphologic diversity of large Martian ripples that helps constrain their formative mechanism. Large ripples develop in isolated fields and on dunes. They form transversely and obliquely to longitudinally to the net sand-flux direction in unimodally and bimodally distributed very fine to very coarse sand. They have either straight or sinuous crestlines. Inactive ripples are covered with dust, whereas migrating ripples are dust free. Here we present a unifying view of ripples that form in near-bed sediment-transport conditions (encompassing fluid-drag and coarse-grained ripples) to explain the range of large-Martian-ripple morphologies and expand the use of bedforms as environmental indicators.

Plain Language Summary Large sand ripples with meter-scale crest-to-crest spacings abound on the Martian surface but are not found in terrestrial sandy deserts. Along its traverse through the Bagnold Dune Field, the Curiosity rover witnessed a rich diversity of such large ripples, both in terms of their shape and of their behavior. Rover observations help understand how these mysterious large Martian ripples form. Here we present a unifying view of ripples that form when grains are mobilized near the sediment bed by various fluids and across planets. Such an understanding of the formation mechanics of similar ripples will enable scientists to use the ripples' imprints on landscapes and in rocks to infer modern and past environmental conditions.

1. Introduction

Wind has shaped the Martian landscape for much of its history and continues to play a major role today (Bridges et al., 2014; Chojnacki et al., 2018; Hayward et al., 2007). Wind-blown bedforms cover much of the modern Martian landscape and signal the dominance of winds as a geomorphic agent on Mars (supporting information Figure S1a). Sand dunes, the largest bedforms, grow to hundreds of meters in wavelength and actively migrate with sand fluxes similar to those of some terrestrial dunes (Ayoub et al., 2014; Bridges et al., 2012, 2017; Chojnacki et al., 2011, 2015; Silvestro et al., 2010, 2013). Smaller bedforms with crest-to-crest wavelengths between ~1 and ~5 m are readily observable from orbit and are ubiquitous on Mars (e.g., Figure S1c; Bridges et al., 2007; Lapotre et al., 2016). Ripples with ~1- to 5-m wavelengths, hereafter referred to as *large Martian ripples*, actively migrate on larger dunes or in sand sheets. Large Martian ripples do not have clear terrestrial analogs and their formation mechanisms remain poorly understood. They have been proposed to be analogous to the more familiar decimeter-scale terrestrial impact ripples (Almeida et al., 2008; Durán et al., 2014) or a different type of bedform altogether (Lapotre et al., 2016).

Ground observations of eolian bedforms occurred soon after the Mars Exploration Rovers landed in 2004 (Greeley et al., 2004; Sullivan et al., 2005, 2008). The Spirit rover observed decimeter-scale ripples migrating on top of meter-scale ripples that made up a sand sheet at El Dorado (Sullivan et al., 2008). The Mars Exploration Rovers also observed coarse-grained ripples, armored with grains >2 mm in diameter and lacking superimposed smaller ripples (Jerolmack et al., 2006; Sullivan et al., 2008). Along its traverse through a two-phase scientific campaign at the Bagnold Dunes (Bridges & Ehlmann, 2018; Lapotre & Rampe, 2018), Curiosity made detailed observations of a diverse suite of eolian bedforms—small ripples

migrating over large ripples, which in turn migrate over larger dunes (Ewing et al., 2017; Lapotre et al., 2016), as well as isolated large ripples and coarse-grained ripples (see Table S1 for a summary of ripple characteristics).

In this manuscript, we supplement observations made during Phase 1 of the campaign (Ewing et al., 2017; Lapotre et al., 2016) with new data acquired during Phase 2 and review the morphology, dynamics, grain size, and activity of bedforms encountered along Curiosity's traverse through the Bagnold Dunes (Figure S1b; Table S1) as it pertains to understanding the formation of large Martian ripples in fine mono-disperse sand (i.e., sand with a unimodal and narrow grain-size distribution). Altogether, observations from the campaign further support the idea that large Martian ripples are a class of bedform distinct from impact ripples. Based on a comparison between large Martian ripples and a suite of candidate analog terrestrial bedforms that share similar morphologies and dynamics, we propose that large Martian ripples belong to a family of bedforms that form across fluids and planets when a significant fraction of the sediments is transported near their threshold of motion and close to the bed.

2. Morphologic Diversity of Ripples Observed by Curiosity at Gale Crater

2.1. The Size Gap Between Small and Large Ripples

Phase 1 of the Bagnold Dunes campaign showed the coexistence of three distinct bedform-wavelength populations: decimeter-scale ripples superimposed on the stoss slope of meter-scale ripples that were themselves superimposed on decameter-scale barchan dunes (Figure 1a; Lapotre et al., 2016). Orbital measurements of bedform wavelengths from 11 Martian dune fields combined with rover measurements of small and large Martian ripples demonstrated the presence of three main distinct bedform modes across Mars (Figure 1a; Lapotre et al., 2016). Orbital and ground data sets overlap in the ~0.8- to 3-m range, demonstrating the continuity of the compilation across scales. No bedforms within the ~20- to 80-cm wavelength range were found in monodisperse sand during the campaign, suggesting that small and large ripples form two distinct wavelength populations.

2.2. Morphology and Dynamics of Large Ripples

During the campaign, large Martian ripples were found in isolated ripples fields (Lapotre & Rampe, 2018; Weitz et al., 2018) and on top of dunes (Ewing et al., 2017; Lapotre et al., 2016). Large ripples found on the stoss slopes of both Namib and High Dunes (Figure S1b for location) had highly sinuous crests and asymmetric profiles (Figures 1a and 1e). This morphology differed significantly from the straight crests and more symmetric profiles of small ripples superimposed on the large ripples (Figure 1; Table S1) and from the straight-crested large ripples formed along the steep primary and secondary lee slopes of Namib Dune (Ewing et al., 2017). The straight crests of the small ripples are consistent with impact ripples (Table S1) and the straight-crested large ripples formed on steep slopes are consistent with straightening by gravitationally driven along-crest transport (Rubin, 2012). The slip faces of large ripples displayed grainfall, grainflow, and deflected small ripples, none of which are present on smaller ripples (Figure 1b). Ubiquitous lee-slope grainfall indicates settling of sand out of suspension past ripple crests, grainflow indicates lee-slope oversteepening and subsequent avalanching, and deflected ripples indicate secondary lee-slope winds (Figure 1b). All demonstrate the strong feedback between winds and ripple topography. With the exception of few longitudinal ripples in the horns of Namib Dune (morphologic analog to longitudinal spurs, Figure S2a; Ewing et al., 2017), large ripples observed from the ground prior to Phase 2 formed primarily transverse (with a possible oblique component, e.g., Silvestro et al., 2016) to the net sandflux direction. Longitudinal (or oblique) ripples, however, were identified from orbit further south within the Bagnold Dunes (Ewing et al., 2017; Silvestro et al., 2016).

At the Mapleton site (Phase 2; Figure S1b for location), Curiosity observed a set of straight-crested large ripples, with typical wavelengths of ~2 m (Figures 1c and 1e). There, the crests of large ripples were oriented longitudinally to the axis of the Nathan Bridges Dune (039–042° and 042–045° for the dune and ripples, respectively), which formed either longitudinally or obliquely to the net sand-flux direction (Figure S1b; Silvestro et al., 2016). The Mapleton large ripples (Figure 1c) were morphologically different from large ripples formed on High and Namib Dunes (Table S1). They lacked slip faces, grainfall and grainflow deposits, and have much more symmetric profiles (Figures 1c and 1e). Large ripples were covered with small ripples migrating along the large-ripple crests (Figure 1c). The small ripples near the crests on the NW-facing sides were
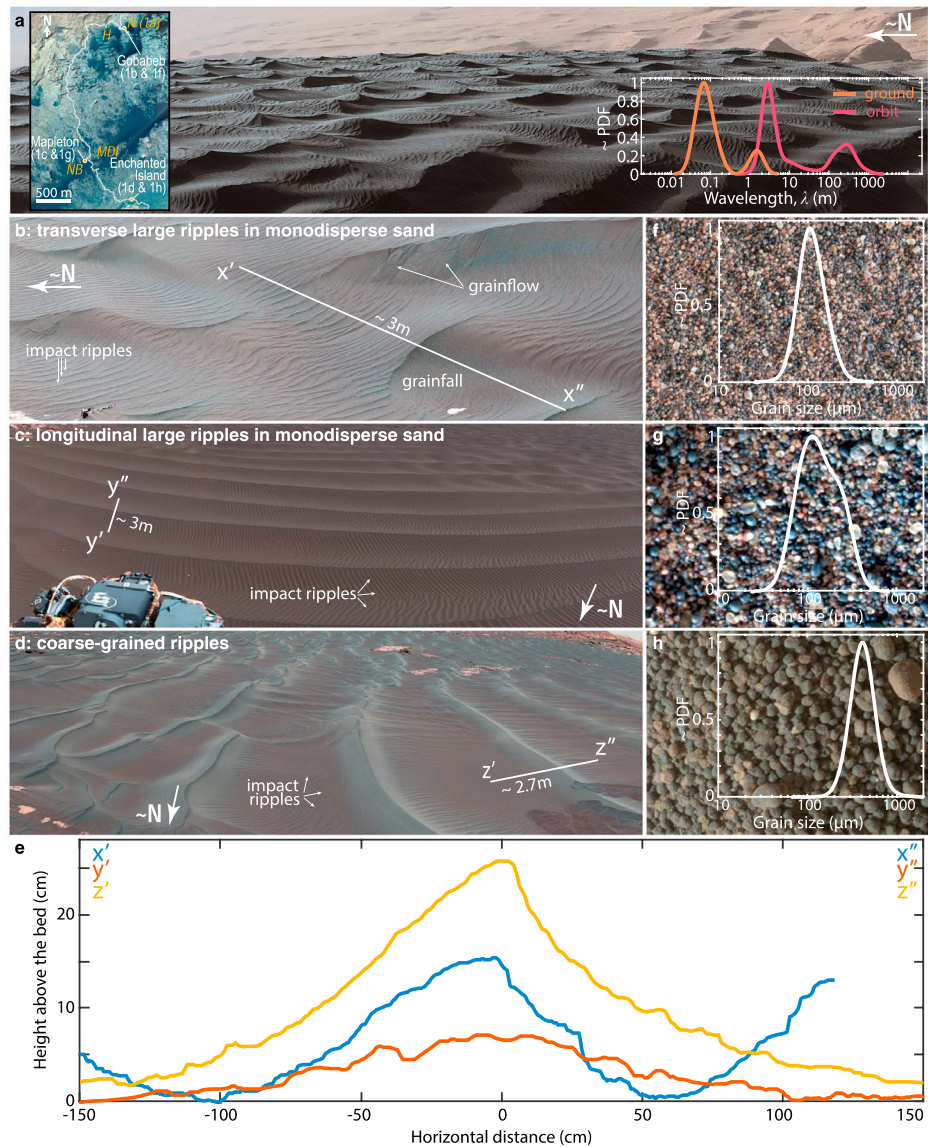
Figure 1. (a) Mosaic of Mast Camera (Mastcam) images (mcam005410, sol 1192) showing two scales of ripples on the stoss slope of Namib Dune. Left inset shows an overview map of Curiosity's traverse through the Bagnold Dunes centered on 4°42'00" S, 137°21'30" E (N = Namib Dune, H = High Dune, NB = Nathan Bridges Dune, MDI = Mount Desert Island; see Figure S1b for a more detailed map with location names). Right inset shows the wavelength distribution of Martian eolian bedforms, combining ground and orbital measurements (Lapotre et al., 2016). Note that whereas magnitude of the probability density functions (PDFs) cannot be compared across data sets, peaks within each data set allow the identification of three distinct wavelength modes. (b) Mastcam mosaic (mcam005597, sol 1221) of large transverse ripples showing grainfall, grainflows, and deflected small ripples at the Gobabeb site on Namib Dune (Figures S1b and S1c). (c) Mastcam mosaic (mcam008154, sol 1601) of large longitudinal ripples at the Mapleton site on the Nathan Bridges Dune (Figure S1b). (d) Mastcam mosaic (mcam009157, sol 1752) of transverse coarse-grained ripples at the Enchanted Island site (Figure S1b). There, rare coarse-grained ripples were observed with wavelengths in the ~20- to 80-cm range (near the image center). (e) Profiles of a large transverse ripple at Gobabeb (x'-x"; Figure 1b; Figures S1b and S1c for location), a large longitudinal ripple at Mapleton (y'-y"; Figure 1c), and a coarse-grained ripple at Enchanted Island (z'-z"; Figure 1d). The Gobabeb profile was derived from a digital elevation model built from Mastcam stereopairs, whereas the Mapleton and Enchanted Island digital elevation models were generated from Navigation Cameras stereopairs. All profiles were median-filtered with a 10-cm window size. (f) Mars Hand Lens Imager (MAHLI) image (1242MH0005740000403707R00, sol 1242) of sand grains at a ripple crest at Gobabeb (Otavi target), with kernel density of grain size overlain. (g) MAHLI image (1604MH0004580000602124R00, sol 1604) of sand grains at a ripple crest at Mapleton (Flume Ridge target), with kernel density of grain size overlain. (h) MAHLI image (1751MH0007220000700514R00, sol 1751) of sand grains at a ripple crest at Enchanted Island, with kernel density of grain size overlain. Panels (f)–(h) are exactly 1 cm across their width, allowing for direct visual comparison of grains between the three sites. Grain-size data are presented in Weitz et al. (2018).

perpendicular to the large-ripple crests but changed orientation to oblique in the troughs and up the SE-facing sides of the large ripples (Figure 1c). This indicates that the last formative wind for small ripples was from the NE direction and that they were responding to the secondary flows induced by large-ripple topography. Despite interactions between small ripples and large-ripple crests, the latter remained sharp and clearly defined, indicating that small impact ripples are part of the formative process rather than reworking larger ripples (Figure 1c). We thus interpret that the large, straight-crested ripples formed longitudinally (or obliquely) to the net sand-flux direction, consistent with previous orbital inferences (Silvestro et al., 2013, 2016).

2.3. Grain Sizes and Bedform Activity

Orbiter-based observations suggest that Martian dunes are composed of coarse sand (Edgett & Christensen, 1991; Pelkey & Jakosky, 2002). However, in the actively migrating transverse and longitudinal large ripples at the Bagnold Dunes, rover measurements using the Mars Hand Lens Imager (MAHLI) indicated very-fine-to-fine sand (median 100–150 μm; Figures 1f and 1g; Ehlmann et al., 2017; Ewing et al., 2017; Weitz et al., 2018), and previous estimates from midinfrared spectroscopy likely overestimated grain size due to subpixel sand/bedrock mixing (Edwards et al., 2018). One large ripple at the base of the stoss slope of High Dune consisted of medium sand (median $\approx$ 350 μm) at its crest. Larger grains are expected at the base of High Dune because it occurs at the deflationary, trailing edge of the dune field where coarse grains should concentrate (Ewing et al., 2017; Lapotre et al., 2016). High Dune is also surrounded by bedrock on which larger grains could readily move (Baker, Newman, et al., 2018) until coming to rest at the base of the sandy, steeper dune stoss slope. Grain-size measurements performed along the crests of isolated ripples or in ripple fields south of the Bagnold Dunes (e.g., Figure 1d; Figure S1b for location) displayed medium sand (~300–500 μm; Figure 1h). The coarsest grains were measured at the crest of the Schoolhouse Ledge isolated ripple (median $\approx$ 480 μm with ~1% grains >1 mm; Figure S1b; Weitz et al., 2018).

Although MAHLI cannot resolve individual dust grains, fine Martian dust has elevated S and Cl contents, which are detectable by the Alpha Particle X-Ray Spectrometer (APXS) and ChemCam instruments (Ehlmann et al., 2017; Lasue et al., 2018). The active sands of Gobabeb and Ogunquit Beach (Figure S1b for location) are depleted in H, S, and Cl compared with previously analyzed Martian regolith and sand (e.g., Leshin et al., 2013). This indicates very low to no dust within active dune sands (Cousin et al., 2017; Ehlmann et al., 2017; Gabriel et al., 2018; O'Connell-Cooper et al., 2017, 2018; Stern et al., 2018) and corroborates orbital and rover spectral observations of sand (Johnson et al., 2017, 2018; Lapotre, Ehlmann, et al., 2017). In contrast to active ripples, some coarse-crested isolated large ripples and ripple fields display a thin veneer of dust aggregates with elevated H, S, and Cl, indicating they have not been recently active (O'Connell-Cooper et al., 2018; Weitz et al., 2018).

High Resolution Imaging Science Experiment (HiRISE) images showed both large transverse ripples and dunes migrating at rates of ~0.1–1.7 m/Earth year and ~0.2 m/Earth year, respectively, near the rover traverse (Bridges et al., 2017; Silvestro et al., 2013, 2016). The relatively low sand-flux associated with both large-ripple and dune migration is consistent with transport near the impact threshold (section 4.2; Baker, Lapotre, et al., 2018). Eolian activity, as determined from orbit (Ayoub et al., 2014), and in situ from the motion of coarse grains on bedrock along Curiosity's traverse (Baker, Newman, et al., 2018), is greatest during southern summer when Mars is near perihelion. Consistent with this observation, Phase 1 of the campaign occurred just after aphelion during southern fall to winter, and frequent and repeated sol-to-sol observations of eolian bedforms did not show significant changes. Rather, rare grain scrambling, two centimeter-scale grainflows, and one centimeter-scale slump were observed over the course of ~3 months (Bridges et al., 2017).

No direct observations of ripple migration were made during Phase 1 of the campaign, which raises the question of the timing of movement of the large and small ripples. However, several observations indicate that the ripples migrate coevally. For example, grainflows that downlap onto small ripples deflected along a large-ripple lee slope indicate large-ripple lee-slope activity during small-ripple migration (Figure 1b), and in some areas, small and large ripples formed in the same orientation, implying the same formative wind direction (Ewing et al., 2017; Lapotre et al., 2016). Further, large ripples have been observed from orbit to migrate seasonally near perihelion (Ayoub et al., 2014), and, during Phase 2 of the campaign, which occurred near perihelion, the small ripples were observed to migrate at rates of the order of a few centimeters per sol (Baker, Lapotre, et al., 2018), thus demonstrating the cooccurrence of both small and large-ripple migration near perihelion. Notably, the lack of reworking of large-ripple crests by small ripples during Phase 2 suggests that the small ripples contribute to the overall morphology and migration of the large ripples.

3. Terrestrial Analogs to Large Martian Ripples

The observed diversity and complex behavior of large Martian ripples is not typically recognized in terrestrial eolian ripples (e.g., Lapotre et al., 2016; Silvestro et al., 2016; Vaz et al., 2017), and as such, they do not have clear terrestrial analogs. Morphometric characteristics of bedforms are commonly used to constrain their formation processes (Ashley, 1990; Werner et al., 1986; Zimbelman et al., 2012). Here we present the morphometric characteristics of four bedform types as a baseline to identify potential terrestrial analogs to large Martian ripples and constrain their formation mechanism.

3.1. Subaqueous Ripples

3.1.1. Morphology

Current ripples form in sand under unidirectional currents in water. They have equilibrium wavelengths of ~10–20 cm in freshwater and are distinct from larger, meter-scale fluvial dunes (Ashley, 1990; Lapotre, Lamb, et al., 2017). Current ripples have complex, typically three-dimensional and sinuous crestlines (Figure 2a; Rubin & McCulloch, 1980; Southard & Boguchwal, 1990) and asymmetric profiles (Figure 2f) that resemble those of transverse large Martian ripples (Figures 1a, 1b, and 1e; section 2.2). In contrast, wave ripples form in bidirectional (reversing) flows and typically have linear crestlines and symmetric profiles (Figures 2b and 2f; Miller & Komar, 1980), morphologically (but not dynamically; section 4.1) similar to those of longitudinal large Martian ripples (Figures 1c and 1e; section 2.2).

3.1.2. Formation

Subaqueous ripples are often referred to as *drag ripples* because they form in response to a spatial lag between the loci of maximum fluid shear stress, maximum sand flux, and bed topography (Charru et al., 2013; Richards, 1980; Smith, 1970). Current ripples form at low particle Reynolds numbers (Re_p) and Shields stresses (τ_*) (Southard & Boguchwal, 1990; Van den Berg & Van Gelder, 2009), typically under bedload-transport conditions (Richards, 1980) in laminar (with respect to Re_p; Engelund & Hansen, 1967) and hydraulically smooth (Nikuradse, 1933) flows. However, current-ripple-stability boundaries do not directly coincide with bedload/suspension, laminar/turbulent, or smooth/rough transitions (Lapotre, Lamb, et al., 2017). Lapotre, Lamb, et al. (2017) proposed that the stability and equilibrium wavelength of current ripples (λ) can be predicted from grain diameter (D), sediment specific submerged weight (Rg, where $R = \frac{\rho_s - \rho_f}{\rho_f}$, and ρ_s and ρ_f are sediment and fluid densities, respectively), fluid shear velocity (u_*), and fluid kinematic viscosity (ν) through a relationship between the Yalin number, $\chi = Re_p \tau_*^{1/2} \propto \frac{L_{sat} u_*}{\nu}$ (with $Re_p = \frac{u_* D}{\nu}$ and $\tau_* = \frac{u_*^2}{RgD}$), and a dimensionless wavelength, $\lambda^* = \frac{\lambda u_*}{\nu}$. Dimensionless wavelength can be envisioned as a ripple-scale Reynolds number and χ as a Reynolds number where the length scale is proportional to a saturation length, L_{sat} (Lapotre, Lamb, et al., 2017), which was shown to control the initial wavelength of current ripples (Charru et al., 2013). From a comprehensive data compilation, Lapotre, Lamb, et al. (2017) showed that ripples form for $\chi < \sim 4 - 9$, and that in that regime

$$\lambda^* \approx 2500\chi^{1/3}, \tag{1}$$

or in dimensional form,

$$\lambda \approx 2500 \frac{\nu^{2/3} D^{1/6}}{(Rg)^{1/6} u_*^{1/3}}. \tag{2}$$

Importantly, equation (2) shows that fluid density affects drag-ripple wavelength through its effect on fluid kinematic viscosity (Grazer, 1982; Lamb, Grotzinger, et al., 2012) and specific submerged density of the sediment and that λ decreases when ρ_f increases.

Finally, the geometry of subaqueous ripples forming under varying flow directions is a function of the time the bedform takes to adjust to changes in flow direction (and thus a function of its volume relative to the volume of sediment transported during individual flow events; Rubin & Ikeda, 1990). For example, in the case of orbital wave ripples (i.e., those wave ripples with wavelengths proportional to wave-oscillation amplitude near the bed) without superimposed net current, ripple wavelength varies with sediment and fluid properties as well as wave frequency and near-bed maximum wave orbital velocity (Pedocchi & García, 2009b, 2009a).
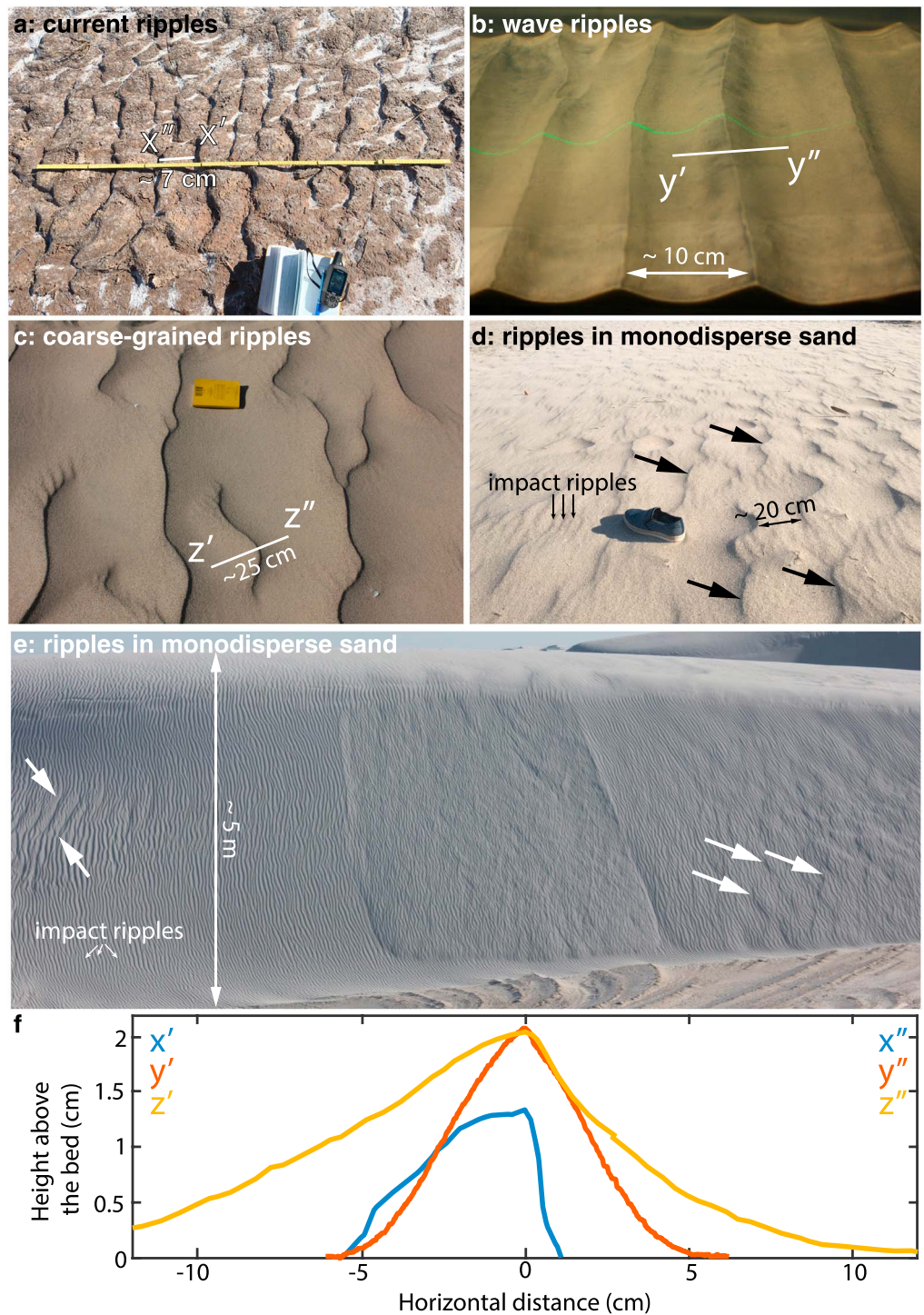
Figure 2. Terrestrial analogs to large Martian ripples. (a) Current ripples from a dry riverbed in Death Valley, California. (b) Orbital wave ripples created in a flume experiment (Nienhuis et al., 2014; Perron et al., 2016). (c) Coarse-grained ripples from Oceano Dunes, California. (d) Damp beach ripples, Playa del Rey, California. (e) Large sinuous ripples forming on the lee slope of a dune at White Sands National Monument, New Mexico. In (d) and (e), large ripples are highlighted with large one-sided arrows. (f) Profiles of a current ripple (x'-x"; Figure 2a), a wave ripple (y'-y"; Figure 2b), and a coarse-grained ripple (z'-z"; Figure 2c). Profiles x'-x" and z'-z" were derived from digital elevation models built using the structure from motion technique with Agisoft software, whereas profile y'-y" was derived through image analysis using a laser sheet by Nienhuis et al. (2014).

3.2. Coarse-Grained Ripples
3.2.1. Morphology

Coarse-grained ripples (also known as megaripples) are eolian bedforms that form at a wide range of wavelengths (~20 cm to >300 m) and only arise in polydisperse beds (Figure 2c; Bagnold, 1941; Lämmel et al., 2018; Yizhaq et al., 2009). Whereas most grains in the troughs of coarse-grained ripples are comprised of fine sand, coarser grains (typically ~2–4 mm on Earth) concentrate along sometimes complex, sinuous, three-dimensional crestlines (Bagnold, 1941; Sharp, 1963; Yizhaq et al., 2012), similar to those of transverse large Martian ripples (Figures 1a and 1b). Like large Martian ripples and Martian coarse-grained ripples (Figure 1e), terrestrial coarse-grained ripples may have symmetrical or asymmetrical profiles (Figure 2f) and may be oblique relative to the net sand-transport direction where they form in response to bimodal winds. Owing to their apparent morphologic similarity, coarse-grained ripples were invoked as possible analogs for meter-scale Martian bedforms observed from orbit (De Silva et al., 2013).

3.2.2. Formation

The stability and formation of coarse-grained ripples require (i) a bimodal grain-size distribution, and (ii) wind speeds high enough for fine grains to saltate but low enough for the coarser fraction of grains to only be mobilized by surface creep through saltation impact (Bagnold, 1941; Yizhaq et al., 2009). Under these conditions, fine and coarse grains may segregate, and local coarsening of the bed leads to the slow formation of coarse-grained ripples (Ellwood et al., 1975; Sharp, 1963; Yizhaq et al., 2009). As long as wind speeds do not exceed the saltation threshold for coarse grains, coarse-grained ripples may grow indefinitely; however, coarse-grained ripples break down to smaller impact ripples if wind speeds temporarily exceed the threshold of saltation for coarse grains (Bagnold, 1941; Yizhaq et al., 2009). Because of their dune-like size-dependent shape and the predicted existence of a minimum coarse-grained-ripple size described by a saturation length scale, coarse-grained ripples were proposed to be *reptation dunes* (Lämmel et al., 2018).

3.3. Terrestrial Ripples in Monodisperse Sand
3.3.1. Morphology

Bagnold (1941) first described a peculiar set of sinuous transverse eolian ripples that only formed within restricted experimental conditions in very fine sand at similar wavelengths or slightly larger wavelengths than the more familiar impact ripples (~15–20 cm). These ripples had long gentle stoss slopes and shorter, steeper lee slopes. Wilson (1972) later identified rogue ripples in the field that may be analogous to Bagnold's ripples but formed primarily longitudinally to the net sand flux. However, to our knowledge, similar bedforms have not been subsequently recognized or described. In Figures 2d and 2e, we identified terrestrial decimeter-scale sinuous and asymmetric ripples that formed in monodisperse sand. These bedforms appear to share striking morphologic and dynamic similarity with large Martian ripples (Figures 1a and 1b).

3.3.2. Formation

Bagnold (1941) hypothesized that his sinuous eolian ripples form analogously to current ripples, making them eolian drag ripples. Wilson (1972) referred to his longitudinal counterparts to Bagnold's ripples as *aerodynamic ripples*, by analogy to the hydrodynamic mechanism responsible for current- and wave-ripple formation. However, wind-drag ripples are not commonly recognized and described in terrestrial sandy deserts, and their existence should be debated. The crestline geometry of ripples shown in Figures 2d and 2e is difficult to explain through an impact mechanism, which would straighten the crests through lateral splash in monodisperse sand (Rubin, 2012). Thus, we propose that these bedforms are candidate terrestrial wind-drag ripples. Interestingly, equation (2) predicts that terrestrial wind-drag ripples would form at wavelengths of ~10–20 cm, consistent with Bagnold's experiment and the terrestrial sinuous transverse ripples in fine sand shown in Figures 2d and 2e.

4. Discussion: A Ripple Continuum Forming Under Near-Bed Transport Conditions
4.1. The Wind-Drag Formation Hypothesis for Large Martian Ripples

On the basis of (i) distinct sizes, (ii) disparate morphologies, and (iii) coeval formation in very-fine-to-fine sand, Lapotre et al. (2016) concluded that small Martian ripples and large Martian ripples must form from different mechanisms. Lapotre et al. (2016) argued that large Martian ripples are wind-drag ripples in recognition of the apparent role played by atmospheric kinematic viscosity in controlling their wavelength. Building on morphometric characteristics of large Martian ripples and their propensity to migrate both transversely and longitudinally, Silvestro et al. (2016) and Vaz et al. (2017) further concluded that the dynamics of large

ripples conflict with those of terrestrial impact ripples, such that large Martian ripples may be more analogous to eolian dunes than impact ripples. Longitudinal bedforms on Earth form underwater and subaerially owing to locally reversing flows (Figure S2). Longitudinal eolian ripples on Earth are rare but do occur in the lee of obstacles (Figures S2b and S2c) in response to high-frequency vortex shedding and turbulence, and their crestline orientation reflects time-averaged lee-side wind conditions. Importantly, whether transverse or longitudinal, those bedforms that form in bidirectional flows tend to have symmetric profiles (e.g., Figures 2b and 2f; Rubin, 2012; Rubin & Ikeda, 1990), similar to those of longitudinal large Martian ripples (Figure 1e). Thus, the symmetric profiles of longitudinal large Martian ripples are consistent with a formation under changing wind directions. However, whereas, for example, wave ripples form from reversing flows within timescales of seconds to minutes, large-Martian-ripple formation may integrate winds with divergence angles between 90° and 180° over diurnal-to-seasonal changes in wind direction (Ewing et al., 2017). We propose that these longer timescales and the larger volumes of sediments involved in reorienting a whole bedform (e.g., Rubin & Ikeda, 1990) allow for the formation of longitudinal large Martian ripples through the same wind-drag mechanism proposed for the formation of transverse large Martian ripples.

Further elaborating on the work of Lapotre, Lamb, et al. (2017), Durán et al. (2017) proposed that both current and large Martian ripples form at low λ^* (analogous to the wind-drag hypothesis of Lapotre et al. (2016), and consistent with Lapotre, Lamb, et al. (2017)) under hydrodynamically smooth conditions, whereas impact ripples form under hydrodynamically rough conditions. They expanded the Yalin number ($\chi \propto \frac{L_{sat} u_*}{\nu}$) formulation of Lapotre, Lamb, et al. (2017) by using different formulations for the saturation length for transports in bedload and saltation, respectively. Hamidouche et al. (2018) further showed that a transition in the behavior of the recirculation zone and reattachment point past a drag-ripple crest occurs at $\lambda^* \approx 5000$ (i.e., $\chi \approx 8$), consistent with the stability of drag ripples as predicted by Lapotre, Lamb, et al. (2017). Thus, under the wind-drag model, (i) large Martian ripples and impact ripples are not genetically related, (ii) large Martian ripples and current ripples belong to a then yet undescribed bedform family that may form under water and winds, and (iii) drag-ripple size varies with kinematic viscosity (equation (2)). Importantly, conditions that lead to drag-ripple formation are promoted under thick viscous sublayers, that is, for high-kinematic-viscosity flows and/or low flow velocities. A key observation that strongly supports this argument and would need to be explained by any other model is the presence of clearly defined wavelengths associated with impact ripples and large ripples. Intermediate-scale, compound ripples in the ~20- to 80-cm wavelength range were notably absent in monodisperse sands throughout the Bagnold Dunes campaign. The only bedforms of intermediate scale that were found clearly displayed coarse crests (Figures 1d and 1h; Weitz et al., 2018), have wavelengths consistent with the predicted minimum size of coarse-grained ripples on Mars (Lämmel et al., 2018), and are thus interpreted as coarse-grained ripples.

4.2. Near-Bed-Transport Bedforms Across Fluids on Earth and Mars

As described in sections 2 and 3, large Martian ripples, current ripples, coarse-grained ripples, and terrestrial wind-drag ripples all display sinuous crestlines when they are transverse to a unidirectional flow. All of these bedforms have asymmetric profiles with steep lee slopes, some of which are dominated by slip face processes (grain-flow and/or grainfall). Where forming in bidirectional flows (i.e., excluding current ripples), they are recognized to form longitudinally or obliquely and have more symmetrical profiles. Furthermore, equation (1) readily predicts the size of current ripples (Lapotre, Lamb, et al., 2017), large Martian ripples across a broad range of atmospheric densities (Lapotre et al., 2016), and predicts that terrestrial wind-drag ripples should form at ~10- to 20-cm wavelengths, consistent with Bagnold's experiment and rarely recognized terrestrial sinuous ripples in fine sand (Figures 2d and 2e). On Earth, equation (1) coincidentally predicts wind-drag ripples to be similar in size to large impact ripples, which is also coincidentally similar in size to the smallest terrestrial coarse-grained ripples (Figure 2c; Lämmel et al., 2018).

In addition to morphometric and dynamic similarities (section 3), drag and coarse-grained ripples are unified through their formation in lower-intensity sediment-transport conditions near the threshold of motion, where grains predominantly move near the sediment bed. Specifically, large Martian ripples form under low saltation fluxes at wind speeds near the impact threshold (e.g., Baker, Lapotre, et al., 2018; Sullivan & Kok, 2017); current ripples form under low bed stresses (Richards, 1980), while linear and symmetric wave ripples tend to form in medium-to-coarse sand at lower wave orbital velocities (Lamb, Fischer, et al., 2012; Pedocchi & García, 2009b, 2009a); coarse-grained ripples form through reptation of coarse grains at wind

speeds below their impact threshold (Yizhaq et al., 2009); and our candidate terrestrial wind-drag ripples (Figures 2d and 2e; section 3.3) likely formed under low saltation fluxes. For example, ripples in Figure 2d formed in damp beach sand, where pore water induces cohesion, raising the fluid threshold, and leading to low saltation fluxes. Ripples in Figure 2e formed in angular (raising the fluid threshold) gypsum sand by secondary deflected flows on the lee slope of a dune (where low transport would be expected). Thus, we propose that drag (current and wind) and coarse-grained ripples belong to a broader family of bedforms. Although their modes of sediment transport may differ, these bedforms share similar morphologies, analog dynamics, and sizes that may be predicted by equation (1). Their formation appears to be unified by near-bed transport of a significant fraction of the sediments. On those grounds, we propose that:

1. Large Martian ripples are wind-drag ripples. Their stability is permitted on Mars by the high kinematic viscosity of the low-density Martian atmosphere and near-impact threshold formative wind speeds.
2. Terrestrial sinuous eolian ripples formed in monodisperse sands may also be wind-drag ripples. They are rarely recognized on Earth, and although their abundance remains to be determined, they may be rare due to the restrictive low-Yalin-number condition for their formation.
3. Drag (current and wind on Earth and Mars) and coarse-grained ripples are unified by their formation under near-bed sediment-transport conditions at near-threshold wind speeds.

5. Conclusions

The Curiosity rover documented a variety of eolian bedforms: small impact ripples, large ripples in fine sand, coarse-grained ripples, and dunes. Large ripples, in particular, display diverse morphologies and apparent dynamics: they may be sinuous or straight-crested, fine or coarse-crested, isolated in patches or on dunes, transverse or longitudinal to the net wind direction, active or inactive, and dust free or dusty. On the basis of similar morphologies, analog dynamics, and sizes that are controlled by fluid-drag theory, we propose that large Martian ripples belong to a broader family of bedforms that form under near-bed sediment transport, including drag (water or wind) and coarse-grained ripples. Importantly, because the stability and size of drag ripples are strongly controlled by environmental fluids, the recognition of drag ripples or their cross-stratification enables a quantitative characterization of the environmental conditions under which they formed. Drag-ripple cross-stratification formed by water on Earth and Mars (Lamb, Grotzinger, et al., 2012) and by winds on Mars (Banham et al., 2018; Lapotre et al., 2016) has been previously recognized. Drag ripples may also prove useful quantitative environmental indicators on Venus (e.g., Venusian *microdunes*; Durán et al., 2017; Lorenz & Zimbelman, 2014), Titan (Lapotre, Lamb, et al., 2017), possibly other planetary bodies (e.g., 67P-Churyumov Gerasimenko comet; Jia et al., 2017), but also to interpret the ancient sedimentary record of Earth.

References

Almeida, M. P., Parteli, E. J., Andrade, J. S., & Herrmann, H. J. (2008). Giant saltation on Mars. *Proceedings of the National Academy of Sciences of the United States of America*, *105*(17), 6222–6226. https://doi.org/10.1073/pnas.0800202105

Ashley, G. (1990). Classification of large-scale subaqueous bedforms: A new look at an old problem. SEPM bedforms and bedding structures. *Journal of Sedimentary Research*, *60*(1), 160–172.

Ayoub, F., Avouac, J.-P., Newman, C., Richardson, M., Lucas, A., Leprince, S., & Bridges, N. (2014). Threshold for sand mobility on Mars calibrated from seasonal variations of sand flux. *Nature Communications*, *5*(1), 5096. https://doi.org/10.1038/ncomms6096

Bagnold, R. (1941). *The physics of blown sand and desert dunes*. London: Courier Corporation.

Baker, M., Lapotre, M., Bridges, N., Minitti, M., Newman, C., Ehlmann, B., et al. (2018). The Bagnold Dunes in southern summer: Active sediment transport on Mars observed by the Curiosity rover. *Geophysical Research Letters*, https://doi.org/10.1029/2018GL079040

Baker, M. M., Lapotre, M. G. A., Minitti, M. E., Newman, C. E., Sullivan, R., Weitz, C. M., et al. (2018). Coarse sediment transport in the modern Martian environment. *Journal of Geophysical Research: Planets*, *123*, 1380–1394. https://doi.org/10.1002/2017JE005513

Banham, S. G., Gupta, S., Rubin, D. M., Watkins, J. A., Sumner, D. Y., Edgett, K. S., et al. (2018). Ancient Martian aeolian processes and palaeomorphology reconstructed from the Stimson formation on the lower slope of Aeolis Mons, Gale crater, Mars. *Sedimentology*, *65*(4), 993–1042. https://doi.org/10.1111/sed.12469

Bridges, N., Ayoub, F., Avouac, J., Leprince, S., Lucas, A., & Mattson, S. (2012). Earth-like sand fluxes on Mars. *Nature*, *485*(7398), 339–342. https://doi.org/10.1038/nature11022

Bridges, N., Calef, F., Hallet, B., Herkenhoff, K., Lanza, N., Le Mouélic, S., et al. (2014). The rock abrasion record at Gale crater: Mars Science Laboratory results from Bradbury landing to Rocknest. *Journal of Geophysical Research: Planets*, *119*, 1374–1389. https://doi.org/10.1002/2013JE004579

Bridges, N., & Ehlmann, B. (2018). The Mars Science Laboratory (MSL) Bagnold Dunes campaign, Phase I: Overview and introduction to the special issue. *Journal of Geophysical Research: Planets*, *123*, 3–19. https://doi.org/10.1002/2017JE005401

Bridges, N., Geissler, P., McEwen, A., Thomson, B., Chuang, F., Herkenhoff, K., et al. (2007). Windy Mars: A dynamic planet as seen by the HiRISE camera. *Geophysical Research Letters*, *34*, L23205. https://doi.org/10.1029/2007GL031445

Bridges, N., Sullivan, R., Newman, C., Navarro, S., Van Beek, J., Ewing, R., et al. (2017). Martian aeolian activity at the Bagnold Dunes, Gale Crater: The view from the surface and orbit. *Journal of Geophysical Research: Planets*, *122*, 2077–2110. https://doi.org/10.1002/2017JE005263

Charru, F., Andreotti, B., & Claudin, P. (2013). Sand ripples and dunes. *Annual Review of Fluid Mechanics*, *45*(1), 469–493. https://doi.org/10.1146/annurev-fluid-011212-140806

Chojnacki, M., Banks, M., & Urso, A. (2018). Wind-driven erosion and exposure potential at Mars 2020 rover candidate-landing sites. *Journal of Geophysical Research: Planets*, *123*, 468–488. https://doi.org/10.1002/2017JE005460

Chojnacki, M., Burr, D., Moersch, J., & Michaels, T. (2011). Orbital observations of contemporary dune activity in Endeavor crater, Meridiani Planum, Mars. *Journal of Geophysical Research*, *116*, E00F19. https://doi.org/10.1029/2010JE003675

Chojnacki, M., Johnson, J., Moersch, J., Fenton, L., Michaels, T., & Bell, J. (2015). Persistent aeolian activity at Endeavour crater, Meridiani Planum, Mars; new observations from orbit and the surface. *Icarus*, *251*, 275–290. https://doi.org/10.1016/j.icarus.2014.04.044

Cousin, A., Dehouck, E., Meslin, P. Y., Forni, O., Williams, A. J., Stein, N., et al. (2017). Geochemistry of the Bagnold dune field as observed by ChemCam and comparison with other aeolian deposits at Gale Crater. *Journal of Geophysical Research: Planets*, *122*, 2144–2162. https://doi.org/10.1002/2017JE005261

De Silva, S., Spagnuolo, M., Bridges, N., & Zimbelman, J. (2013). Gravel-mantled megaripples of the Argentinean Puna: A model for their origin and growth with implications for Mars. *GSA Bulletin*, *125*(11–12), 1912–1929. https://doi.org/10.1130/B30916.1

Durán, O., Andreotti, B., Claudin, P., & Winter, C. (2017). A unified model of bedforms in water, Earth, and other planetary bodies, Paper presented at American Geophysical Union Fall Meeting, AGU, New Orleans, LA.

Durán, O., Claudin, P., & Andreotti, B. (2014). Direct numerical simulations of aeolian sand ripples. *Proceedings of the National Academy of Sciences of the United States of America*, *111*, 15,665–15,668. https://doi.org/10.1073/pnas.1413058111

Edgett, K., & Christensen, P. (1991). The particle size of Martian aeolian dunes. *Journal of Geophysical Research*, *96*(E5), 22,765–22,776. https://doi.org/10.1029/91JE02412

Edwards, C., Piqueux, S., Hamilton, V., Fergason, R., Herkenhoff, K., Vasavada, A., et al. (2018). The thermophysical properties of the Bagnold Dunes, Mars: Ground-truthing orbital data. *Journal of Geophysical Research: Planets*, *123*, 1307–1326. https://doi.org/10.1029/2017JE005501

Ehlmann, B., Edgett, K., Sutter, B., Achilles, C., Litvak, M., Lapotre, M., et al. (2017). Chemistry, mineralogy, and grain properties at Namib and High dunes, Bagnold dune field, Gale crater, Mars: A synthesis of Curiosity rover observations. *Journal of Geophysical Research: Planets*, *122*, 2510–2543. https://doi.org/10.1002/2017JE005267

Ellwood, J., Evans, P., & Wilson, I. (1975). Small scale aeolian bedforms. *Journal of Sedimentary Research*, *45*(2), 554–561.

Engelund, F., & Hansen, E. (1967). A monograph on sediment transport in alluvial streams, Technical University of Denmark Ostervoldgade 10, Copenhagen K.

Ewing, R., Lapotre, M., Lewis, K., Day, M., Stein, N., Rubin, D., et al. (2017). Sedimentary processes of the Bagnold Dunes: Implications for the eolian rock record of Mars. *Journal of Geophysical Research: Planets*, *122*, 2544–2573. https://doi.org/10.1002/2017JE005324

Gabriel, T. S. J., Hardgrove, C., Czarnecki, S., Rampe, E., Rapin, W., Achilles, C. N., et al. (2018). Water abundance of dunes in Gale Crater, Mars from active neutron experiments and implications for amorphous phases. *Geophysical Research Letters*. https://doi.org/10.1029/2018GL079045

Grazer, R. (1982). *Experimental study of current ripples using medium silt*. Cambridge, MA: Massachusetts Institute of Technology

Greeley, R., Squyres, S., Arvidson, R., Bartlett, P., Bell, J., Blaney, D., et al. (2004). Wind-related processes detected by the Spirit rover at Gusev Crater, Mars. *Science*, *305*(5685), 810–813. https://doi.org/10.1126/science.1100108

Hamidouche, S., Calluaud, D., Pineau, G., & Texier, A. (2018). Study of instantaneous flow behind a single fixed ripple. *Journal of Hydro-Environment Research*, *19*, 117–127. https://doi.org/10.1016/j.jher.2018.03.002

Hayward, R. K., Mullins, K. F., Fenton, L. K., Hare, T. M., Titus, T. N., Bourke, M. C., et al. (2007). Mars global digital dune database and initial science results. *Journal of Geophysical Research*, *112*, E11007. https://doi.org/10.1029/2007JE002943

Jerolmack, D., Mohrig, D., Grotzinger, J., Fike, D., & Watters, W. (2006). Spatial grain size sorting in eolian ripples and estimation of wind conditions on planetary surfaces: Application to Meridiani Planum, Mars. *Journal of Geophysical Research*, *111*, E12S02. https://doi.org/10.1029/2005JE002544

Jia, P., Andreotti, B., & Claudin, P. (2017). Giant ripples on comet 67P/Churyumov–Gerasimenko sculpted by sunset thermal wind. *Proceedings of the National Academy of Sciences of the United States of America*, *114*(10), 2509–2514. https://doi.org/10.1073/pnas.1612176114

Johnson, J., Achilles, C., Bell, J., Bender, S., Cloutis, E., Ehlmann, B., et al. (2017). Visible/near-infrared spectral diversity from in situ observations of the Bagnold Dune Field sands in Gale Crater, Mars. *Journal of Geophysical Research: Planets*, *122*, 2655–2684. https://doi.org/10.1002/2016JE005187

Johnson, J. R., Bell, J. F. III, Bender, S., Cloutis, E., Ehlmann, B., Fraeman, A., et al. (2018). Bagnold Dunes campaign Phase 2: Visible/near-infrared reflectance spectroscopy of longitudinal ripple sands. *Geophysical Research Letters*. https://doi.org/10.1029/2018GL079025

Lamb, M., Grotzinger, J., Southard, J., & Tosca, N. (2012). Were aqueous ripples on Mars formed by flowing brines? Rep. 1565763122, pp. 139–150, SEPM Special Publication, Tulsa, OK.

Lamb, M. P., Fischer, W. W., Raub, T. D., Perron, J. T., & Myrow, P. M. (2012). Origin of giant wave ripples in snowball Earth cap carbonate. *Geology*, *40*(9), 827–830. https://doi.org/10.1130/G33093.1

Lämmel, M., Meiwald, A., Yizhaq, H., Tsoar, H., Katra, I., & Kroy, K. (2018). Aeolian sand sorting and megaripple formation. *Nature Physics*, *14*(7), 759–765. https://doi.org/10.1038/s41567-018-0106-z

Lapotre, M., Ehlmann, B., Minson, S., Arvidson, R., Ayoub, F., Fraeman, A., et al. (2017). Compositional variations in sands of the Bagnold Dunes, Gale crater, Mars, from visible-shortwave infrared spectroscopy and comparison with ground truth from the Curiosity rover. *Journal of Geophysical Research: Planets*, *122*, 2489–2509. https://doi.org/10.1002/2016JE005133

Lapotre, M., Lamb, M., & McElroy, B. (2017). What sets the size of current ripples? *Geology*, *45*(3), 243–246. https://doi.org/10.1130/G38598.1

Lapotre, M., & Rampe, E. (2018). Curiosity's investigation of the Bagnold Dunes, Gale crater: Overview of the two-phase scientific campaign and introduction to the special collection. *Geophysical Research Letters*. https://doi.org/10.1029/2018GL079032

Lapotre, M. G. A., Ewing, R. C., Lamb, M. P., Fischer, W. W., Grotzinger, J. P., Rubin, D. M., et al. (2016). Large wind ripples on Mars: A record of atmospheric evolution. *Science*, *353*(6294), 55–58. https://doi.org/10.1126/science.aaf3206

Lasue, J., Cousin, A., Meslin, P.-Y., Mangold, N., Wiens, R. C., Berger, G., et al. (2018). Martian eolian dust probed by ChemCam. *Geophysical Research Letters*. https://doi.org/10.1029/2018GL079210

Leshin, L. A., Mahaffy, P. R., Webster, C. R., Cabane, M., Coll, P., Conrad, P. G., et al. (2013). Volatile, isotope, and organic analysis of martian fines with the Mars Curiosity rover. *Science*, *341*(6153). https://doi.org/10.1126/science.1238937

Lorenz, R., & Zimbelman, J. (2014). *Dune worlds: How wind-blown sand shapes planetary landscapes*. New York: Praxis-Springer.

Miller, M., & Komar, P. (1980). Oscillation sand ripples generated by laboratory apparatus. *Journal of Sedimentary Research*, *50*(1), 173–182.

Nienhuis, J., Perron, J., Kao, J., & Myrow, P. (2014). Wavelength selection and symmetry breaking in orbital wave ripples. *Journal of Geophysical Research: Earth Surface*, *119*, 2239–2257. https://doi.org/10.1002/2014JF003158

Nikuradse, J. (1933). Strömungsgesetz in rauhen Rohren. *Rep.*, pp. 22.

O'Connell-Cooper, C., Spray, J., Thompson, L., Gellert, R., Berger, J., Boyd, N., et al. (2017). APXS-derived chemistry of the Bagnold dune sands: Comparisons with Gale crater soils and the global Martian average. *Journal of Geophysical Research: Planets*, *122*, 2623–2643. https://doi.org/10.1002/2017JE005268

O'Connell-Cooper, C. D., Thompson, L. M., Spray, J. G., Berger, J. A., VanBommel, S. J., Gellert, R., et al. (2018). Chemical diversity of sands within the linear and barchan dunes of the Bagnold Dunes, Gale Crater, as revealed by APXS onboard Curiosity. *Geophysical Research Letters*. https://doi.org/10.1029/2018GL079026

Pedocchi, F., & García, M. (2009a). Ripple morphology under oscillatory flow: 1. Prediction. *Journal of Geophysical Research*, *114*, C12014. https://doi.org/10.1029/2009JC005354

Pedocchi, F., & García, M. (2009b). Ripple morphology under oscillatory flow: 2. Experiments. *Journal of Geophysical Research*, *114*, C12015. https://doi.org/10.1029/2009JC005356

Pelkey, S., & Jakosky, B. (2002). Surficial geologic surveys of Gale Crater and Melas Chasma, Mars: Integration of remote-sensing data. *Icarus*, *160*(2), 228–257. https://doi.org/10.1006/icar.2002.6978

Perron, J., Myrrow, P., Huppert, K., Koss, A., & Wickert, A. (2016). *Wave ripple time-lapse experiments edited*. SEAD Internal Repository. https://doi.org/10.5967/M0QR4V39

Richards, K. (1980). The formation of ripples and dunes on an erodible bed. *Journal of Fluid Mechanics*, *99*(3), 597–618. https://doi.org/10.1017/S002211208000078X

Rubin, D. (2012). A unifying model for planform straightness of ripples and dunes in air and water. *Earth-Science Reviews*, *113*(3–4), 176–185. https://doi.org/10.1016/j.earscirev.2012.03.010

Rubin, D., & Ikeda, H. (1990). Flume experiments on the alignment of transverse, oblique, and longitudinal dunes in directionally varying flows. *Sedimentology*, *37*(4), 673–684. https://doi.org/10.1111/j.1365-3091.1990.tb00628.x

Rubin, D., & McCulloch, D. (1980). Single and superimposed bedforms: A synthesis of San Francisco Bay and flume observations. *Sedimentary Geology*, *26*(1–3), 207–231. https://doi.org/10.1016/0037-0738(80)90012-3

Sharp, R. (1963). Wind ripples. *The Journal of Geology*, *71*(5), 617–636. https://doi.org/10.1086/626936

Silvestro, S., Fenton, L., Vaz, D., Bridges, N., & Ori, G. (2010). Ripple migration and dune activity on Mars: Evidence for dynamic wind processes. *Geophysical Research Letters*, *37*, L20203. https://doi.org/10.1029/2010GL044743

Silvestro, S., Vaz, D., Ewing, R., Rossi, A., Fenton, L., Michaels, T., et al. (2013). Pervasive aeolian activity along rover Curiosity's traverse in Gale Crater, Mars. *Geology*, *41*(4), 483–486. https://doi.org/10.1130/G34162.1

Silvestro, S., Vaz, D., Yizhaq, H., & Esposito, F. (2016). Dune-like dynamic of Martian aeolian large ripples. *Geophysical Research Letters*, *43*, 8384–8389. https://doi.org/10.1002/2016GL070014

Smith, J. (1970). Stability of a sand bed subjected to a shear flow of low Froude number. *Journal of Geophysical Research*, *75*(30), 5928–5940. https://doi.org/10.1029/JC075i030p05928

Southard, J., & Boguchwal, L. (1990). Bed configurations in steady unidirectional water flows. Part 2. Synthesis of flume data. *Journal of Sedimentary Research*, *60*(5), 658–679.

Stern, J. C., Sutter, B., Archer, P. D., Eigenbrode, J. L., McAdam, A. C., Franz, H. B., et al. (2018). Major volatiles evolved from eolian materials in Gale crater. *Geophysical Research Letters*. https://doi.org/10.1029/2018GL079059

Sullivan, R., Arvidson, R., Bell, J., Gellert, R., Golombek, M., Greeley, R., et al. (2008). Wind-driven particle mobility on Mars: Insights from Mars Exploration Rover observations at "El Dorado" and surroundings at Gusev Crater. *Journal of Geophysical Research*, *113*, E06S07. https://doi.org/10.1029/2008JE003101

Sullivan, R., Banfield, D., Bell, J. F., Calvin, W., Fike, D., Golombek, M., et al. (2005). Aeolian processes at the Mars exploration rover Meridiani Planum landing site. *Nature*, *436*(7047), 58–61. https://doi.org/10.1038/nature03641

Sullivan, R., & Kok, J. (2017). Aeolian saltation on Mars at low wind speeds. *Journal of Geophysical Research: Planets*, *122*, 2111–2143. https://doi.org/10.1002/2017JE005275

Van den Berg, J.-I., & Van Gelder, A. (2009). A new bedform stability diagram, with emphasis on the transition of ripples to plane bed in flows over fine sand and silt, Alluvial Sedimentation (Special Publication 17 of the IAS), 66, 11.

Vaz, D., Silvestro, S., Sarmento, P., & Cardinale, M. (2017). Migrating meter-scale bedforms on Martian dark dunes: Are terrestrial aeolian ripples good analogues? *Aeolian Research*, *26*, 101–116. https://doi.org/10.1016/j.aeolia.2016.08.003

Weitz, C., Sullivan, R., Lapotre, M., Rowland, S., Grant, J., Baker, M., & Yingst, R. (2018). Sand grain sizes and shapes in eolian bedforms at Gale Crater, Mars. *Geophysical Research Letters*, https://doi.org/10.1029/2018GL078972

Werner, B., Haff, P., Livi, R., & Anderson, R. (1986). Measurement of eolian sand ripple cross-sectional shapes. *Geology*, *14*(9), 743–745. https://doi.org/10.1130/0091-7613(1986)14<743:MOESRC>2.0.CO;2

Wilson, I. (1972). Aeolian bedforms—Their development and origins. *Sedimentology*, *19*(3–4), 173–210. https://doi.org/10.1111/j.1365-3091.1972.tb00020.x

Yizhaq, H., Isenberg, O., Wenkart, R., Tsoar, H., & Karnieli, A. (2009). Morphology and dynamics of aeolian mega-ripples in Nahal Kasuy, southern Israel. *Israel Journal of Earth Sciences*, *57*, 149–165.

Yizhaq, H., Katra, I., Kok, J., & Isenberg, O. (2012). Transverse instability of megaripples. *Geology*, *40*(5), 459–462. https://doi.org/10.1130/G32995.1

Zimbelman, J., Williams, S., & Johnston, A. (2012). Cross-sectional profiles of sand ripples, megaripples, and dunes: A method for discriminating between formational mechanisms. *Earth Surface Processes and Landforms*, *37*(10), 1120–1125. https://doi.org/10.1002/esp.3243